Thermally stable and polar zwitterionic liquid stationary phases for gas chromatography: Understanding the impact of chemical structure

Victoria R. Zeger[1], Bhawana Thapa[1], Jessica F. DeLair[1], David S. Bell[2], Daniel Shollenberger[3], Moubani Chakraborty[3], Jason S. Herrington[3], and Jared L. Anderson*,[1]

[1] Department of Chemistry, Iowa State University, Ames, Iowa 50011 USA
[2] ASKkPrime LLC, Bellefonte, Pennsylvania 16823, USA
[3] Restek Corporation, 110 Benner Circle, Bellefonte, Pennsylvania 16823, USA

Abstract

The chemical structure of nine imidazolium sulfonate and triflimide zwitterionic liquids (ZILs) were systematically tuned to increase their thermal stability for gas chromatography (GC) separations. Substituents for imidazolium and 2-phenylimidazolium cation systems, comprised of alkyl, benzyl, and oligoether groups of varying chain lengths, were studied as stationary phases in GC. Propanesulfonate, ethanesulfonate, and propanetriflimide anions were examined to understand the effect of linker length and nucleophilicity on ZIL thermal stability. Studies were conducted to assess film stability and thermal lability of ZIL stationary phases on fused silica capillaries when exposed to elevated temperatures for prolonged time periods. All stationary phases exhibited relatively poor film stability on untreated capillary surfaces, but most showed repeatable chromatographic retention after stepwise heating from 100 to 200 °C. To understand the thermal degradation pathways of the ZILs, mass spectrometry (MS) was used to monitor the degradation/volatilization of the stationary phase when heated from 40-250 °C. Salt-deactivated surfaces were effective at mitigating stationary phase instability, but were observed to participate in the degradation of alkyl functionalized ZILs via nucleophilic attack of the alkyl substituent. This was not observed for oligoether substituted ZILs. Imidazolium propanesulfonate ZILs all underwent degradation through the detachment of the anion system, resulting in the reformation of 1,3-propanesultone. Most ZIL stationary phases degraded below 230 °C, but the cation substituent was observed to play a significant role in overall ZIL thermal stability. For the imidazolium propanetriflimide ZIL, degradation of the anion system occurred prior to the detachment of the entire anion system via elimination and occurred at around 245 °C.

*Corresponding author: Jared L. Anderson, Department of Chemistry, Iowa State University. andersoj@iastate.edu

Keywords: gas chromatography; stationary phase; zwitterionic liquid; thermal stability; mass spectrometry.

1. Introduction

Ionic liquids (ILs) have gained considerable attention as green materials and have been applied in the fields of chromatography [1], extractions and sample preparation [2,3], electrochemistry [4,5], mass spectrometry [6], and spectroscopy [7]. Compared to traditional classes of solvents, ILs possess low vapor pressures and higher thermal stabilities, making them particularly useful in high temperature applications [8]. Some of their initial uses as stationary phases in gas chromatography (GC) noted their unique separation selectivity but limited temperature range, 110-160 °C for 1-ethylpyridinium bromide and 40-120 °C for ethylammonium nitrate [1,9]. With the rapid development of room temperature ILs, their tunable physico-chemical properties and wider temperature ranges have made them ideal for imparting selectivity in gas phase separations [8,10], and many studies have sought to understand IL solvation properties by making modifications to their chemical structures [11–13]. In general, it has been observed that changing the anion of ILs affects retention of molecules the most in GC, with finer tuning possible by modifying the substituents of the cation systems. Additionally, anions often have the greatest influence on IL thermal stability, with large anions featuring delocalized charge being the most thermally stable [14]. The higher thermal stability and unique retention of polar IL stationary phases has led to their commercialization as wall-coated open tubular (WCOT) columns.

Zwitterionic liquids (ZILs), a subset of ILs possessing covalently bonded cations and anions, have been applied for cellulose dissolution and as extraction solvents for polar molecules due to their strong hydrogen bonding capability [15,16]. ZILs were also shown to possess higher polarity and stronger hydrogen bonding interactions when compared to traditional IL homologues [17]. In 2018, ZILs were reported as stationary phases in GC for the separation of volatile carboxylic acids, where their strong retention was largely attributed to the high hydrogen bond

basicity of the anionic component [18]. The ZIL columns had higher retention factors and better peak asymmetry factors than commercial polar columns used for fatty acid analysis, offering limited thermal stability (ranging from 200-225 °C) compared to 270-280 °C for commercial WCOT columns. These results have sparked an interest in developing more thermally stable ZIL stationary phases to achieve selectivity of acidic analytes.

It is imperative that GC columns maintain high efficiency over hundreds of heating and cooling cycles for repeatable, well-resolved separations and accurate analyte quantification. When loss of separation efficiency occurs, peaks in chromatograms are observed to broaden, leading to poorly resolved separations and lower signal-to-noise ratios. With substantial peak broadening, it can also be challenging to discriminate peaks from the baseline, resulting in inaccurate peak areas integrations. There are two possible mechanisms responsible for stationary phase instability that result in loss of efficiency in GC. The first mechanism results in a phase rearrangement phenomenon known as Rayleigh instability and the other involves thermal degradation of the phase.

Phase rearrangement is often attributed to a surface energy mismatch between the stationary phase and the capillary surface, leading to poor wetting of the surface and minimization of the solid/liquid interfacial energy. Poor wettability is mainly thought to occur when the surface energy of the capillary surface is below the critical surface tension of the stationary phase [19]. In 1987, Bartle et al. criticized this notion and proposed that phase rearrangement in GC occurs via Rayleigh instability to "decrease the interfacial energy at the liquid/gas interface" [20]. In this case, high efficiency thin films of stationary phases that were initially observed to wet the capillary surface can break apart into low efficiency droplets over time. The theory is dependent not only

on surface tension, but also stationary phase viscosity, film thickness, and the inner diameter of the capillary.

Loss of separation efficiency can also occur due to stationary phase loss from thermal degradation or volatilization, often referred to as column bleed. In this case, molecules or oligomers of the stationary phase may break apart and volatilize as the column is heated to higher temperatures. Significant loss of the stationary phase results in decreased retention factors and increased peak tailing as more of the capillary surface becomes exposed. While increased peak tailing can also result from phase rearrangement, decreased retention factors can only result from a loss of stationary phase. Significant effort has been made in characterizing the thermal stability of ILs through thermogravimetric analysis (TGA) [21–24]. These studies have shown that the degree of thermal stability for cations followed the trend: imidazolium > pyridinium > ammonium. The most thermally stable anions also followed the trend of $[PF_6^-] > [NTf_2^-] > [BF_4^-] > [TfO^-] > [CH_3SO_3^-] > [NO_3^-] > [Br^-] > [Cl^-] > [Ac^-]$. Another study assessed the thermal stability of sulfonic acid ILs and found that methylimidazolium cations were more stable than triethanolammonium and pyridinium cations [25]. While slower temperature ramp rates in TGA are expected to yield more accurate results, it is impractical due to the time needed to conduct one experiment, and thus, analyses are often collected using ramp rates of 5 or 10 °C min^{-1}. While these results are acceptable for general comparisons, they are often in conflict with what is observed when monitoring stationary phase bleed using sensitive chromatographic detectors, resulting in an over-estimation of thermal stability. This is especially true for detectors kept under vacuum, such as GC-MS [26]. Therefore, an understanding of the thermal degradation pathway for ZILs under chromatographically-relevant temperatures and conditions is needed to design more thermally stable stationary phases.

To unravel the thermal degradation mechanism of ILs, studies using various forms of mass spectrometry have been conducted [27–33]. For IL systems containing less nucleophilic halide anions, loss of the alkyl substituent from the cation systems occurred in part through an elimination reaction [34]. When the anions are more nucleophilic, loss of the alkyl substituent was observed to occur through a reverse Menshutkin reaction by nucleophilic halide anions [35]. For ILs with [NTf_2^-] anions, elimination products were more abundant than substitution products and degradation of the anion occurred [28]. By substituting an alkyl substituent for a benzyl moiety, the thermal degradation mechanism may change from a S_N2 to S_N1 pathway, through which a stable carbonium ion forms [36]. One study compared the thermal degradation mechanism of oligoether-containing ILs for those with aliphatic groups using differential scanning calorimetry (DSC) and TGA with infrared spectroscopy (TGA-IR) and noted that the presence of oligoether groups led to a loss of the other alkyl substituent faster than the aliphatic IL [37]. These results suggest that oligoether substituents may form less thermally stable ILs than alkyl substituents. Studies have also explored 2-methylimidazolium cation systems, where increased thermal stability was observed compared to imidazolium cations [38]. While some of these degradation mechanisms may still hold true for ZILs, no study has specifically studied their thermal degradation mechanisms and the role that restricted motion of the cation and anion systems plays in their thermal stability.

This study explores both fundamental aspects of thermal stability with the intention of designing thermally stable ZILs for use as GC stationary phases. Nine imidazolium sulfonate and [NTf_2^-]-based ZILs were systematically modified to identify key functional groups/substituents that influence ZIL thermal stability. Octyl, decyl, benzyl, and oligoether (OE) substituents were investigated using imidazolium and 2-phenylimidazolium cation systems. Ethanesulfonate (C_2S),

propanesulfonate (C_3S), and (propylsulfonyl)((trifluoromethyl)sulfonyl)imide (C_3NTf) anions were also examined. In some cases, modifications to the capillary were made to alter the surface energy of the inner capillary surface through the deposition of salt onto the capillary wall [19], [39]. In this process, the deposited salt crystals provide a roughened surface that allows for more interactions with the stationary phase material and provides a more uniform and stable coating. This study also discusses the effects that salt treated surfaces have on stationary phase rearrangement and thermal degradation for both alkyl and oligoether functionalized ZILs. The knowledge and understanding of degradation mechanisms obtained in this study aids in guiding the design of more thermally stable ZILs to meet the high temperature requirements of GC.

2. Experimental

2.1 Materials and Reagents

The following reagents were used in the synthesis of ZIL stationary phases. Triethylamine (≥99.5%), 1,3-propanesultone (98%), potassium hydroxide (>90%), 1H-imidazole (99%), 1-benzylimidazole (99%), triethylene glycol monomethyl ether (m-PEG-3) (≥97%), diethylene glycol monomethyl ether (m-PEG-2), hexanes (≥98.5%), ethyl acetate (≥99.5%), and methanol (≥99.9%) were purchased from Sigma-Aldrich (St. Louis, MO, USA). Acrylonitrile (≥99%) and 1-bromooctane (99%) were obtained from Aldrich Chemical Company. Sodium 2-bromoethanesulfonate (98%), methane sulfonyl chloride (98%), sodium hydroxide (98%), and 2-phenylimidazole (98%) were purchased from Thermo Scientific (Waltham, MA, USA) while dichloromethane (≥99.5%), acetone (≥99.5%), acetonitrile (≥99.95%), and dimethyl sulfoxide (>99.9%) were from Fisher Scientific (Waltham, MA, USA). Additional reagents including 1-octylimidazole (>98.0%) from Tokyo Chemical Industry (TCI) (Tokyo, Japan), 1-octylimidazole (99.90%) from AmBeed (Arlington Hts., IL, USA), 1-bromodecane (>98%) from TCI, and 1,2-

dichloroethane (≥99%) from Alfa Aesar (Ward Hill, MA, USA) were obtained. Deuterated NMR solvents were either from Sigma-Aldrich (chloroform and heavy water) or Cambridge Isotope Laboratory Incorporated (dimethyl sulfoxide) (Tewskbury, MA, USA). Untreated capillary tubing (60 m x 0.25 mm i.d.) was obtained from Restek Corporation (Bellefonte, PA, USA) and PTFE (0.012 ± 0.001 i.d.) tubing was obtained from Zeus (Orangeburg, SC, USA). Gases used in the operation of GC-FID and GC-MS instruments included ultra-high purity helium, ultra-high purity hydrogen, and Grade D breathing air from Matheson Tri-Gas (Irving, TX, USA). Standards for studying the maximum allowable operating temperature of the stationary phase included 1000 μg mL^{-1} solutions of benzyl alcohol (Sigma-Aldrich, ≥99%) in 1,2-dichloroethane and propionic acid (Sigma-Aldrich, ~99%) in acetonitrile.

2.2 Instrumentation

Characterization of ZIL purity was accomplished using a Bruker Avance Neo 400 nuclear magnetic resonance (NMR) spectrometer and a Varian MR 400 spectrometer to collect ^{1}H and ^{13}C NMR spectra. A Gay Lussac bottle and stopper (2.0 ± 0.1 mL) from Corning Incorporated Life Sciences was used to obtain density measurements of the ZILs via the pycnometer method. The melting points of solid zwitterionic materials at room temperature were obtained using a MelTemp apparatus and alcohol thermometer to confirm IL properties. Water baths equipped with a thermal regulator and vacuum pump system, shown in Figure S1 of the supplementary information (SI), were used to prepare 5 m GC columns. For efficiency determination, retention measurements, and maximum allowable operating temperature (MAOT) studies, an Agilent 6890 gas chromatograph, equipped with a 7683B automatic liquid sampler and a flame ionization detector (GC-FID), was used. To construct stationary phase bleed profiles, an Agilent 6890 GC with a 5977A electron ionization mass spectrometer (EI-MS) was used.

174 2.3 Synthesis of Zwitterionic Liquids

175 All ZIL synthesis procedures and conditions can be found in the SI. Reaction progression
176 was monitored daily using ^{1}H NMR. All final products were characterized using ^{1}H and ^{13}C
177 NMR.

178 2.4 Coating of Capillary Columns

179 WCOT columns were prepared using the static coating method. All coating solutions for
180 PEG-based stationary phases were prepared using a solvent mixture of 8% (v/v) solution of
181 methanol in dichloromethane (DCM). Coating solutions for stationary phases comprised of alkyl
182 imidazolium ZILs were prepared using a solvent mixture consisting of 0-5% (v/v) solutions of
183 methanol in DCM. All 5 m columns were coated at 45 °C and 23 inHg. Salt-deactivated capillary
184 tubing was prepared following a previously reported method [39] and were subsequently coated
185 using the static coating method.

186 2.5 Conditions for Testing Column Efficiency

187 All columns were conditioned at 100 °C for 1 h prior to assessing efficiency. To test column
188 efficiency, 1 µL of a 1000 µg mL^{-1} standard solution of benzyl alcohol in 1,2-dichloroethane was
189 injected with a 20:1 split ratio and was carried out under the isothermal conditions listed in Table
190 1.

191 2.6 Maximum Allowable Operating Temperature Studies

192 MAOTs were determined using a similar method reported by Nan et al. [18]. Retention
193 data for propionic acid and benzyl alcohol were obtained in triplicate under isothermal conditions
194 (Tables S1 and S2) prior to baking the column at various temperatures. The column was initially
195 conditioned for one hour at 125 °C, followed by an isothermal separation of propionic acid and an
196 isothermal separation of benzyl alcohol at 100 °C. Subsequent baking steps were conducted at 150,

175, 200, 225, and 250 °C; all baking steps were followed by isothermal separations of propionic acid and benzyl alcohol at 100 °C. GC conditions for baking the column are listed in Table 2.

2.7 Thermal Degradation Experiments using GC-MS

Bleed profiles for the ZIL columns were obtained by increasing the oven temperature from 40 °C to 250 °C at a ramp rate of 0.5 °C min^{-1}. A 5 m ZIL-coated column was attached to a 30 m segment of empty capillary via a capillary connector; the other end of the empty capillary was placed in the inlet and the coated capillary was fed through the transfer line of the MS. For the C_8ImC_3S-Salt phase, a 20 m segment was cut and installed into the GC-MS without an additional empty capillary. The GC inlet was held at 250 °C and the transfer line held at 280 °C. The MS source and quadrupole were held at 230 and 150 °C, respectively. Other GC conditions used for the stationary phase bleed study consisted of a split ratio of 20:1, flow rate of 1 mL min^{-1}, and UHP helium as the carrier gas.

3. Results and Discussion

3.1 Design of ZIL chemical structures

To study the thermal stability of ZILs, nine ZILs with systematically tuned substituents were designed based on those that have previously shown good separation selectivity as GC stationary phases [18]. Chemical structures of the ZILs are shown in Figure 1 with their respective abbreviations. Since ZILs possess tethered cations and anions, Figure 2 further breaks down the ZIL chemical structure into their respective cation and anion systems for clarity. The cation system refers to the positively charged imidazolium ring and its non-ionic sidechain or substituent; the anion system refers to the negatively charged sulfonate or triflimide anion and the propane linker that tethers it to the cation. Imidazolium cations are known for their vast structural tunability and relatively high thermal stability compared to other cation systems, making them ideal to explore

many different substituents. ZILs containing octyl and decyl sidechains (i.e., C_8ImC_3S and $C_{10}ImC_3S$) and oligoether sidechains of OE_2 and OE_3 (i.e., OE_2ImC_3S and OE_3ImC_3S) were chosen to determine the effect of substituent chain length on thermal stability. The effect of polarity on thermal stability can be assessed by comparing the $C_{10}ImC_3S$ and OE_3ImC_3S ZILs, which possess substituents featuring 10 atoms in the chain. A previous study compared zwitterion number densities and molecular packing information obtained using small- and wide-angle x-ray scattering of aliphatic and oligoether imidazolium sulfonate ZILs, concluding that oligoether ZILs exhibited more homogenous packing due to dipole interactions between the lone pair electrons of oxygen atoms and the cation system [40]. Thus, oligoether groups increase the polarity of ZILs due to their ability to participate in dipole-dipole interactions, as opposed to their alkyl counterparts. The effect of aromaticity on ZIL thermal stability was also explored by incorporating benzyl and phenyl moieties into the ZIL chemical structure. Benzyl groups were previously shown to increase the thermal stability of traditional ILs [41]. A phenyl substituent on the C2 carbon of the imidazolium cation may be expected to hinder the loss of linear substituents by nucleophilic attack due to steric effects. Lastly, studying the C_8ImC_2S and C_8ImC_3NTf ZILs allowed the effect of the anion system on thermal stability to be explored. Traditional ILs comprised of [NTf_2^-] anions have higher thermal stability than ILs with methanesulfonate anions [23]. The effects of linker chain length on thermal stability were also evaluated.

As stated previously, GC stationary phases should exist in a liquid state during separations to facilitate an absorptive mechanism. Highly viscous ZILs that are liquids at room temperature are generally ideal as GC stationary phases. Of the nine ZILs examined in this study, only four can be considered as room temperature ZILs; these being C_8ImC_3S, C_8ImC_2S, OE_2ImC_3S, and OE_3ImC_3S. Melting points for the other stationary phases are presented in Table 3. Photos of all

ZILs are shown in Figure S2a. Appending oligoether substituents to the ZIL chemical structure was observed to significantly reduce their melting points. Specifically, the C_8(Ph)ImC_3S zwitterions did not melt prior to undergoing thermal degradation at 190 °C, as evidenced by the white powder that transformed into a clear liquid and an immiscible orange liquid of equal volume (see Figure S2b). The orange liquid is believed to be the reformed C_8(Ph)Im reactant, whereas the clear liquid is the reformed 1,3-propanesultone in a melted state. However, the OE_3(Ph)ImC_3S ZIL had a melting point range of 92-98 °C, roughly 95 °C below the degradation temperature of the C_8(Ph)ImC_3S zwitterion. Additionally, when the substituent was changed from the n-octyl group to the aromatic benzyl group consisting of an equal number of carbon atoms, the Bz ImC_3S zwitterion was able to withstand temperatures up to 230 °C without melting or degrading. This is in striking contrast to the C_8ImC_3S ZIL that exists as a liquid at room temperature and can likely be explained by the strong intermolecular forces and dense packing of planar aromatic molecules. Additionally, the waxy C_{10}ImC_3S ZIL had a melting point range of 82-85 °C, whereas the OE_3ImC_3S ZIL exists as a liquid at room temperature. The substituent groups appear to increase the melting points of ZILs in the following order: aromatic > alkyl > oligoether.

3.2 Stationary Phase Rearrangement at Elevated Temperatures

One aspect of stationary phase stability often overlooked in GC is the ability of the molecules to rearrange themselves into more thermodynamically favored orientations. As such, thin films of a stationary phase on the capillary wall are transformed into spherical droplets to minimize the surface area to volume ratio, resulting in efficiency losses that can occur over multiple heating and cooling cycles. To monitor this effect, MAOT studies were performed for capillary columns by baking at 125, 150, 175, 200, and 250 °C for 1 h and subsequently cooling to 100 °C. Results from these studies are summarized in Table 4 and the full data sets can be found in Tables S1 and S2.

Chromatograms are also reported in the SI for each ZIL stationary phase studied (Figures S3-8), showing changes in retention, peak shape, and peak width for benzyl alcohol and/or propionic acid after each heating step. Additional chromatograms are provided showing the increased background from ZIL columns that are caused by the elevated temperatures. The probes benzyl alcohol and propionic acid were chosen due to their high retention factors and propensity for secondary interactions with surface silanols on untreated capillary columns. Since rearrangement does not result in stationary phase loss, it is expected that the retention times and calculated retention factors should only be slightly altered due to additional interactions with the newly exposed silanol surface. In such cases, rearrangement of the stationary phase on the capillary wall is thought to occur at temperatures after which column efficiency decreased without an obvious drop in retention factor. However, in cases where both the column efficiency and retention factor decreased, the stationary phase is thought to have undergone thermal degradation. The onset of stationary phase rearrangement was determined to be the temperature after which the measured efficiency for benzyl alcohol and/or propionic acid dropped by $\geq$ 200 plates m^{-1} from an initial efficiency measurement at 100 °C. Often, a continuous drop in efficiency was observed after each heating step until loss of retention was observed. The MAOT for a particular ZIL stationary phase was determined to be the recorded temperature prior to a measurable decrease in retention factor for benzyl alcohol or propionic acid. For the C_8ImC_3S and $C_{10}ImC_3S$ ZIL stationary phases on untreated capillary, benzyl alcohol was observed to increase in retention after the heating cycles. Therefore, the probe molecule with the most consistent retention factors was used to determine values reported in Table 4. For most ZILs, propionic acid and benzyl alcohol were observed to show similar trends in terms of efficiency and retention factor throughout the experiments.

All ZIL stationary phases appeared to suffer from Rayleigh instability to some degree on the surface of untreated capillary and had MAOT values at or above 200 °C. Two stationary phases also exhibited poor stability even at 100 °C; therefore, their MAOT values were not determined. The C_8ImC_3NTf ZIL exhibited a loss of efficiency upon sitting overnight at room temperature. In the case of the OE_3ImC_3S ZIL, the efficiency of benzyl alcohol dropped from 2200 to 1100 plates m^{-1} after heating at 100 °C for approximately 12 h. For oligoether substituted ZILs, the chain length played an important role in the ZIL's propensity to undergo rearrangement with OE_3ImC_3S being less stable than the OE_2ImC_3S ZIL on the untreated capillary surface and is likely due to the decrease in viscosity that was observed previously for imidazolium sulfonate ZILs when the oligoether substituents are increased in length [40,42]. However, by using a salt-deactivated capillary in which a layer of sodium chloride is deposited prior to coating the stationary phase, the OE_3ImC_3S ZIL was able to resist phase rearrangement with only small drops in efficiency observed. Increased stability was also observed for the C_8ImC_3S ZIL coated on a salt surface. Additionally, ZILs that were solid at room temperature (i.e., $C_{10}ImC_3S$, C_8ImC_3NTf, and $OE_3(Ph)ImC_3S$) produced lower efficiency columns on untreated capillary compared to room temperature ZILs. In these cases, it is unclear if the observed loss in efficiency is due to Rayleigh instability or poor wettability.

As the stationary phase undergoes rearrangement and produces droplets, the silanol or salt surface can be exposed and participate in adsorptive-type interactions with probe molecules. Therefore, tailing peaks would be expected for benzyl alcohol and propionic acid. Increased peak asymmetry factors were observed for both probes on oligoether ZIL stationary phases as the efficiency was observed to decrease. Adsorptive hydrogen bonding interactions with the exposed silica or support surface can increase peak asymmetry factors and confirm stationary phase

311 rearrangement and loss of the thin film coating. Interestingly, the peak asymmetry factors for
312 benzyl alcohol were quite large compared to propionic acid on the C_8ImC_3S ZIL columns, and this
313 was not observed for any other ZIL stationary phase, in which peak asymmetry factors mostly
314 ranged from 0.9-2.0. Peak asymmetry factors for benzyl alcohol were also observed to increase as
315 the efficiency dropped and more of the capillary surface because exposed. Improvements in peak
316 asymmetry factors for the salt surface may be due to the deactivation that occurs when the salt is
317 deposited. Conversely, propionic acid had slightly higher peak asymmetry factors on the C_8ImC_3S-
318 Salt column than on the C_8ImC_3S column featuring an untreated capillary surface. Additional
319 adsorptive-type interactions with the salt surface may have produced the increased peak
320 asymmetry factors for propionic acid, although not as significant as those observed for benzyl
321 alcohol on untreated capillary columns.

322 3.3 Thermal degradation of ZILs

323 To better understand ZIL thermal degradation, columns containing ZIL stationary phases
324 were subjected to elevated temperatures and mass spectrometry was employed to measure their
325 thermal degradation products. By assessing the thermal stability in this manner, the suitability of
326 a particular stationary phase for GC and GC-MS analysis can be better determined and the bleed
327 temperature compared to the degradation temperature measured by thermogravimetric analysis
328 (TGA) [26]. Previous studies have shown that higher temperature ramp rates used during TGA
329 provide higher T_{onset} values for ILs compared to slow ramp rates due to shorter exposure times
330 [24]. Since GC separations often require either lower temperature ramp rates and/or temperature
331 holds, TGA data collected using fast ramp rates (i.e., 10 K min^{-1}) often do not match the thermal
332 stabilities observed in separation studies. For this reason, a slow temperature ramp rate of 0.5 °C
333 min^{-1} was chosen to obtain the most accurate T_{bleed}, at which the column bleed was observed to

reach an order of magnitude increase in counts using scan mode. Additionally, results from TGA measure the bulk material whereas a bleed profile using GC-MS studies a thin film of the stationary phase on a fused silica surface under constant flow of an inert gas using a highly sensitive detector. Bleed profiles and the corresponding T_{bleed} temperatures obtained in this study are shown in Figure 3.

It is well understood that the thermal stability of ILs is highly dependent on the anion component [21]. Substitution of the sulfonate anion for the [NTf_2^-]-based anion was observed to increase the thermal stability by approximately 16 °C. Similar observations were made when ILs comprised of methanesulfonate anions were compared to ILs with [NTf_2^-] anions, attributing their higher thermal stability to the reduced basicity and lower nucleophilicity of the anion [23]. The C_8ImC_3S ZIL appeared to be more thermally stable (by approximately 35 °C) than the $C_{10}ImC_3S$ ZIL on untreated capillary. However, only a slight increase in the T_{bleed} temperature was observed for OE_2ImC_3S compared to the OE_3ImC_3S ZIL. While the chain length may significantly affect the thermal stability of alkyl substituents, this effect appears to be minimal for oligoether substituents. By exchanging the octyl moiety for the benzyl group, the thermal stability was significantly increased such that the bleed profile never crossed the T_{bleed} threshold set at 10^6. This is consistent with previous observations made during the melting point experiments and with the literature, where a 45 °C increase in thermal stability was noted for the 1-benzyl-3-methylimidazolium triflate IL compared to the 1-butyl-3-methylimidazolium triflate IL [41]. By incorporating a phenyl moiety in place of a hydrogen at the C2 position of the imidazolium cation, an increase in ZIL thermal stability was expected due to increased steric hindrance preventing degradation via an anion substitution pathway, as observed previously by Cao and Mu with a methyl group [22]. In this case, the opposite was observed and the thermal stability decreased by

approximately 20 °C compared to the OE_3ImC_3S ZIL on untreated capillary. Similarly, thermal degradation observed at 190 °C during the melting point experiments for the $C_8(Ph)ImC_3S$ ZIL suggests that the phenyl moiety in the C2 position further reduced the thermal stability of ZILs. In this case, the positioning of the aromatic moiety within the ZIL chemical structure plays a significant role in modulating thermal stability.

By analyzing mass spectra obtained upon heating the ZILs to elevated temperatures, thermal degradation products providing insight into ZIL thermal degradation mechanisms were identified. Major thermal degradation products and their respective fragments are listed in Table 5. The mass spectra were acquired at 411-412 min (or 245.5-246 °C) to ensure a high signal-to-noise ratio, which resulted in reduced background peaks from the polyimide coating of the capillary, which were identified as ions possessing a mass-to-charge ratios (m/z) of 98 and 99 with almost equal intensity. The mass spectra are shown in Figures S9-S17. No peaks were observed for the ZIL molecular ion except for the C_8ImC_3NTf ZIL at lower temperatures, as shown in Figure S9. The group of ions in the mass spectrum with the highest m/z were considered to belong to the molecular ion of a thermal degradation product. Isotopic ratios were used to determine the chemical formula and fragment ions were then assigned based on known fragmentation pathways. In almost all cases, these ions were determined to originate from substituted imidazole precursors resulting from a loss of the propanesulfonate anion. Ions that were unaccounted for were thought to belong to other degradation products. Ions with m/z values corresponding to those observed in the mass spectrum for 1,3-propanesultone in the National Institute of Standards and Technology (NIST) Webbook database were present in all sulfonate ZILs (mainly 57, 58 and 122 m/z). For these ZILs, substituted imidazoles were likely formed due to nucleophilic attack by the sulfonate anion, resulting in the reformation of 1,3-propanesultone. In Figure S10 for the C_8ImC_3S ZIL, ions

with 180 and 179 m/z were observed and correspond to 1-octylimidazole (C_8Im) and [C_8Im-H]$^+$. Subsequent fragment ions resulted from σ-bond cleavage along the alkyl chain and corresponded to 165, 151, 137, 123, 109, 95, and 81 m/z values in the mass spectrum. An additional peak at 153 m/z was present, which was also believed to be a fragment ion from C_8Im based on the work of Sala et al. [27]. Upon determining possible fragments that could result from the substituted imidazole precursors, the remaining ion peaks were analyzed in a similar manner.

For all ZILs, ions at 96, 82, and 68 m/z may be the result of other significant thermal degradation products or the result of radical site rearrangements [43,44]. In the case of alkyl substituted ZILs, peaks at 55 and 69 m/z in Figures S4 and S5 support the idea of additional thermal degradation products formed via C-C bond cleavage but may also be evidence of the Hofmann elimination product, which results in an alkene being formed from the alkyl substituent. For terminal alkenes, the low m/z fragments (i.e., 70, 56, 55, 43, and 41) are most abundant, making it challenging to discern these products without confirmation by a soft ionization technique [45]. The Hofmann elimination product is a common thermal degradation product for quaternary ammonium compounds and occurs when the anion abstracts a hydrogen atom from a β-carbon. The free radical residing on the β-carbon forms a double bond with the α-carbon, which results in liberation of the alkyl side chain. The elimination mechanism occurs more frequently when the anion is a weak nucleophile [46]. Others have proposed an elimination route occurring from loss of the acidic C2 proton of the imidazolium by the anion that is followed by hydrogen rearrangement with the proton of the β-carbon [47]. In the mass spectrum for the $C_{10}ImC_3S$ ZIL in Figure S11, similar m/z values and respective thermal degradation products were observed, as detailed in Table 5.

For oligoether ZILs (see Figure S12 and S13), the Hofmann elimination product was not evident, but additional thermal degradation products were observed that are thought to result from C-O and/or C-C bond cleavage and hydrogen rearrangement. This homolytic backbone cleavage has been observed previously for polyethylene glycol polymers after pyrolysis by matrix-assisted laser desorption/ionization MS and chemical ionization MS [48]. This mechanism is depicted in Figure 4 for the OE_2ImC_3S ZIL. Similar observations were made for the possible fragments of the OE_3Im thermal degradation product. For the OE_2ImC_3S ZIL, only products from C-O cleavage were observed, but for the OE_3ImC_3S ZIL, C-C bond cleavage products were also observed, with the peak at 126 m/z being most abundant. Some evidence suggests that a second mechanism of ZIL degradation occurs through the elimination of the sulfonate anion. In this case, the resulting product was vinyl sulfonic acid at 108 m/z, which is moderately abundant in the mass spectrum for the OE_2ImC_3S ZIL. The ion peak at 108 m/z was only observed for the OE_2ImC_3S ZIL and suggests that this alternative mechanism does not occur for the OE_3ImC_3S ZIL. For the $OE_3(Ph)ImC_3S$ ZIL, the substituted 2-phenylimidazole product was observed. In Figure S14, these peaks correspond to 290, 275, 259, 245, 231, 215, 213, 201, 187, 171, 157, 103, 89, 77, and 59 m/z. Other thermal degradation products corresponding to homolytic cleavages were observed at 232, 202, 188, 186, 172, 158, 144, and 104 m/z, respectively. The high abundance of the 144 m/z ion corresponding to 2-phenylimidazole (PhIm) indicates that loss of both the cation substituent and anion component occurs readily with the 2-phenylimidazolium cation and may contribute to lower thermal stability. No other alternative thermal degradation products were discerned for the sulfonate anion other than those for 1,3-propanesultone.

For the C_8ImC_3NTf ZIL, the ion with the highest m/z at 364 resulted from the loss of the -CF_3 group. Although exhibiting low abundance at 411 min, this was the most abundant peak at

151 min (before the bleed profile began to deviate from the baseline and significant degradation was observed). In the mass spectrum obtained at 151 min, the molecular ion is present at 433 m/z, indicating that the observed 364 m/z ion is also the most favored fragment formed during ionization. This also suggests that it is more stable, and less energy is required to produce this fragment ion than others [46]. Similar fragmentation was also previously reported for ILs with [NTf_2^-] anions, in which the -CF_3 group facilitated an elimination reaction of the alkyl substituent on the cation system [28]. Since [NTf_2^-] anions are known to have lower nucleophilicity due to their delocalized charge, they are not prone to facilitate degradation via nucleophilic attack. Instead, 77% of IL degradation occurred via an elimination mechanistic pathway [28]. 1-octylimidazole and respective fragment ions were also present, suggesting that the -CF_3 group may have facilitated elimination of the remaining anion component, even though peaks corresponding to the eliminated anion component (i.e., 183, 142, 105, 78 m/z) were not observed. Alternatively, peaks at 253 and 184 m/z suggest that elimination occurs via proton abstraction by the negatively charged nitrogen atom, where fragmentation of the product results in the loss of the -CF_3 group. The higher thermal stability of the C_8ImC_3NTf ZIL may be explained by the larger energy required to facilitate an elimination reaction as opposed to the lower energy required for a nucleophilic attack that occurs with the propanesulfonate anion systems. Regardless of the anion, degradation of ZILs appear to be facilitated by the anion system, although through different degradation pathways. Proposed thermal degradation routes for C_8ImC_3S and C_8ImC_3NTf ZILs are depicted in Figure 5.

In the preparation of select GC columns featuring ZIL stationary phases, sodium chloride was deposited on the capillary surface to mitigate phase rearrangement. To assess the influence of the salt-deactivated surface on ZIL column thermal stability, the C_8ImCS-Salt and OE_3ImC_3S-Salt

448 columns were also subjected to elevated temperatures using GC-MS. Comparison of the mass
449 spectra obtained from C_8ImC_3S-Salt and C_8ImC_3S volatilization/degradation at 411 min showed
450 similar m/z values, except for three ions of high abundance observed at 91, 92, and 93 m/z (see
451 Figure S10). Analysis of the 92 and 93 ion intensities to 91 m/z suggests the presence of a chlorine
452 atom within the molecular structure. The 91 m/z ion was determined to be a fragment resulting
453 from a 1-chlorooctane thermal degradation product, which was noted by McLafferty to be the most
454 abundant peak in mass spectra for larger chloroalkanes ($C_nH_{2n}Cl$, $n \geq 5$) [46]. It has also been
455 previously reported that ILs with chloride anions produce chloroalkane thermal degradation
456 products [24,30]. In one case, the 1-chlorooctane molecular ion was also not detected [30]. The
457 high abundance of this thermal degradation product suggests that this degradation pathway may
458 be the culprit for lower observed T_{bleed} values for the C_8ImC_3S ZIL on salt-deactivated capillary
459 compared to untreated capillary. Similarly, analysis of the mass spectrum in Figure S15 for the
460 C_8ImC_2S ZIL at 412 min indicates the presence of a bromine-containing thermal degradation
461 product based on the isotopic ratios. Since the reaction used to synthesize the ZIL results in a
462 sodium bromide by-product, it is possible that some sodium bromide may remain dissolved in the
463 ZIL after purification. The most abundant ions at 135 and 137 m/z are likely a fragment of a 1-
464 bromooctane thermal degradation product. The T_{bleed} associated with this stationary phase is lower
465 than expected since the short linker length between the cation and anion components should not
466 result in the formation of a cyclic thermal degradation product, which occurs via nucleophilic
467 attack of the sulfonate group, as the resulting 4-membered ring would be rather unstable. However,
468 the presence of a bromide anion could account for this discrepancy, as observed with the C_8ImC_3S
469 ZIL on salt-deactivated and untreated capillary. In this case, the salt-deactivated surface is not a
470 suitable option to prevent stationary phase rearrangement for alkyl ZILs.

Upon comparing the mass spectra for the OE_3ImC_3S-Salt and OE_3ImC_3S columns, no new high abundance ions were observed. The relative intensities of ions at 59 and 89 m/z were observed to mostly increase, as observed in Figure S13. When the mass spectrum from the ZIL coated on untreated capillary was subtracted from the ZIL coated on the salt-deactivated surface (see Figure S16), ion peaks at 59, 89, 63, and 107 m/z were present. The most abundant ion in the subtracted mass spectrum at 63 m/z has a relative abundance of 17.5% compared to the most abundant ion in the mass spectrum for the ZIL on salt-deactivated capillary at 126.1 m/z. The low relative abundance of these additional ions indicates that the formation of this thermal degradation product is less favored, especially compared to the 1-chlorooctane thermal degradation product produced from the C_8ImC_3S-Salt column. This may explain the negligible effect on the T_{bleed} temperature. Deducing the chemical structure of this thermal degradation product is more challenging since the isotopic ratios determined from a subtracted mass spectrum may not be reliable. However, these ions likely result from a thermal degradation product produced by sodium chloride. Since the 59 and 89 m/z ions are fragments of the oligoether sidechain, it is reasonable to suggest that the thermal degradation product is a chlorinated oligoether. Additionally, the 63 and 107 m/z peaks may represent fragment ions with the chemical composition of $C_2H_4Cl^+$ and $C_4H_8ClO^+$, respectively. In this case, salt-deactivated capillary is a reasonable option to mitigate stationary phase rearrangement of the oligoether ZILs as the salt does not appear to readily form chlorinated oligoethers as it does with chloroalkanes.

4. Conclusions

The thermal stabilities of imidazolium sulfonate and triflimide ZILs were investigated to understand the importance of ZIL chemical structure on their thermal degradation mechanism. For GC applications, it is also important for column stationary phases to maintain a thin film on the

wall of the open tubular capillary columns. Of the nine ZILs studied, five were assessed for film stability. All exhibited signs of phase rearrangement based on the loss of column efficiency after extended heating. The OE_3ImC_3S stationary phase was particularly unstable on untreated capillary but was able to maintain high efficiency on a salt-deactivated capillary surface. Improvement in phase stability was also observed for C_8ImC_3S on a salt-deactivated capillary surface. Significant loss of the stationary phase for most ZIL columns occurred after extended heating at 225 °C, putting the MAOT between 200-225 °C as further indicated by drops in analyte retention. To further differentiate ZIL thermal stability, bleed profiles were conducted using GC-MS and suggest that both the cation and anion can play a significant role in modulating ZIL thermal stability. For the imidazolium sulfonate stationary phases, a benzyl moiety afforded the lowest background and highest thermal stability but provides challenges since the zwitterion did not liquify at chromatographically relevant temperatures when observed using a MelTemp apparatus. The oligoether substituents had similar bleed profiles and were also comparable to C_8ImC_3S with thermal stabilities around 225 °C. However, the $C_{10}ImC_3S$ and OE_3(Ph)ImC3S ZILs had reduced thermal stability of approximately 200 °C. To better understand the role C2 substituents and aromatic groups play in ZIL thermal stability, 2-methylimidazolium and benzimidazolium cation systems should be investigated. Additionally, mixed results were observed for ZILs on salt-deactivated surfaces, as the chloride anion of the salt accelerated the thermal degradation of the C_8ImC_3S phase but not the OE_3ImC_3S phase.

Analysis of imidazolium sulfonate ZIL thermal degradation products suggests that most degradation occurs from nucleophilic attack by the sulfonate anion on the α-carbon. When the anion was changed to triflimide, higher thermal stability was achieved and a new thermal degradation mechanism was observed. In this case, degradation of the anion occurred with the loss

517 of the CF_3 group that then facilitated the loss of the remaining anion system via an elimination
518 reaction. This anion system is a promising alternative for high temperature applications, but the
519 high melting point of the C_8ImC_3NTf ZIL makes it less ideal as a GC stationary phase. Based on
520 melting point observations, incorporation of oligoether substituents into the ZIL chemical structure
521 will likely result in reduced melting points to a temperature more amenable for gas-liquid
522 separations. When thermal degradation products of ZILs on salt surfaces were analyzed, the
523 degradation product formed due to the chloride anion for the oligoether ZIL was in much lower
524 abundance than that observed for the alkyl ZIL. Therefore, oligoether substituted imidazolium
525 triflimide ZILs are expected to serve as suitable GC stationary phases as oligoether ZILs are more
526 compatible with different surface modifications and have low melting temperatures while
527 triflimide anions increase ZIL thermal stability.

528 **5. Acknowledgements**

529 The authors acknowledge partial funding of this work through the Chemical Measurement
530 and Imaging Program at the National Science Foundation (Grant No. CHE-2203891). The authors
531 thank Dr. Bruce Richter for his valuable input and discussions.

6. References

[1] F. Pacholec, H.T. Butler, C.F. Poole, Molten organic salt phase for gas-liquid chromatography, Anal. Chem. 54 (1982) 1938–1941. https://doi.org/10.1021/ac00249a006.

[2] J.G. Huddleston, H.D. Willauer, R.P. Swatloski, A.E. Visser, R.D. Rogers, Room temperature ionic liquids as novel media for 'clean' liquid–liquid extraction, Chem Commun (1998) 1765–1766. https://doi.org/10.1039/A803999B.

[3] J. Liu, Y. Chi, G. Jiang, C. Tai, J. Peng, J.-T. Hu, Ionic liquid-based liquid-phase microextraction, a new sample enrichment procedure for liquid chromatography, J. Chromatogr. A 1026 (2004) 143–147. https://doi.org/10.1016/j.chroma.2003.11.005.

[4] J.D. Wadhawan, U. Schroder, A. Neudeck, S.J. Wilkins, R.G. Compton, F. Marken, C.S. Consorti, R.F. de Souza, J. Dupont, Ionic liquid modified electrodes. Unusual partitioning and diffusion effects of Fe(CN)6 4-/3- in droplet and thin layer deposits of 1-methyl-3-(2,6-(S)-dimethylocten-2-yl)-imidazolium tetrafluoroborate, J. Electroanal. Chem. 493 (2000) 75–83. https://doi.org/10.1016/S0022-0728(00)00308-9.

[5] P.B. Hitchcock, T.J. Mohammed, K.R. Seddon, J.A. Zora, l-Methyl-3-ethylimidazolium hexachlorouranate(IV) and I-methyl-3-ethylimidazolium tetrachlorodioxo-uranate(V1): Synthesis, structure, and electrochemistry in a room temperature ionic liquid, Inorg. Chim. Acta 113 (1986) L25–L26. https://doi.org/10.1016/S0020-1693(00)82244-6.

[6] M. Zabet-Moghaddam, E. Heinzle, A. Tholey, Qualitative and quantitative analysis of low molecular weight compounds by ultraviolet matrix-assisted laser desorption/ionization mass spectrometry using ionic liquid matrices, Rapid Commun. Mass Spectrom. 18 (2004) 141–148. https://doi.org/10.1002/rcm.1293.

[7] J. Xia, L. Xia, K. Gong, Y. Liu, W. Liu, G. Wang, X. Su, Preparation of high SERS-active silver films in an aqueous solution of room temperature ionic liquids, Integr. Ferroelectr. 135 (2012) 62–70. https://doi.org/10.1080/10584587.2012.685386.

[8] D.W. Armstrong, L. He, Y.-S. Liu, Examination of ionic liquids and their interaction with molecules, when used as stationary phases in gas chromatography, Anal. Chem. 71 (1999) 3873–3876. https://doi.org/10.1021/ac990443p.

[9] F. Pacholec, C.F. Poole, Stationary phase properties of the organic molten salt ethylpyridinium bromide in gas chromatography, Chromatographia 17 (1983) 370–374. https://doi.org/10.1007/BF02262375.

[10] P. Bonhote, A.-P. Dias, N. Papageorgiou, K. Kalyanasundaram, M. Gra, Hydrophobic, highly conductive ambient-temperature molten salts, Inorg. Chem. 35 (1996) 1168–1178. https://doi.org/10.1021/ic951325x.

[11] M.H. Abraham, W.E. Acree, Jr., Comparative analysis of solvation and selectivity in room temperature ionic liquids using the Abraham linear free energy relationship, Green Chem. 8 (2006) 906. https://doi.org/10.1039/b606279b.

[12] J.L. Anderson, J. Ding, T. Welton, D.W. Armstrong, Characterizing ionic liquids on the basis of multiple solvation interactions, J. Am. Chem. Soc. 124 (2002) 14247–14254. https://doi.org/10.1021/ja028156h.

[13] S.K. Poole, C.F. Poole, Chemometric evaluation of the solvent properties of liquid organic salts, The Analyst 120 (1995) 289. https://doi.org/10.1039/an9952000289.

[14] D.M. Fox, W.H. Awad, J.W. Gilman, P.H. Maupin, H.C. De Long, P.C. Trulove, Flammability, thermal stability, and phase change characteristics of several trialkylimidazolium salts, Green Chem. 5 (2003) 724. https://doi.org/10.1039/b308444b.

[15] K. Kuroda, H. Satria, K. Miyamura, Y. Tsuge, K. Ninomiya, K. Takahashi, Design of wall-destructive but membrane-compatible solvents, J. Am. Chem. Soc. 139 (2017) 16052–16055. https://doi.org/10.1021/jacs.7b08914.
[16] I. Pacheco-Fernández, M.J. Trujillo-Rodríguez, K. Kuroda, A.L. Holen, M.B. Jensen, J.L. Anderson, Zwitterionic polymeric ionic liquid-based sorbent coatings in solid phase microextraction for the determination of short chain free fatty acids, Talanta 200 (2019) 415–423. https://doi.org/10.1016/j.talanta.2019.03.073.
[17] D. Moreno, M. Gonzalez-Miquel, V.R. Ferro, J. Palomar, Molecular and thermodynamic properties of zwitterions versus ionic liquids: A comprehensive computational analysis to develop advanced separation processes, ChemPhysChem 19 (2018) 801–815. https://doi.org/10.1002/cphc.201701093.
[18] H. Nan, K. Kuroda, K. Takahashi, J.L. Anderson, Examining the unique retention behavior of volatile carboxylic acids in gas chromatography using zwitterionic liquid stationary phases, J. Chromatogr. A 1603 (2019) 288–296. https://doi.org/10.1016/j.chroma.2019.06.021.
[19] G. Alexander, Surface characteristics of treated glasses for the preparation of glass capillary columns in gas-liquid chromatography, J Chromatogr. 99 (1974) 81–101. https://doi.org/10.1016/S0021-9673(00)90848-3.
[20] K.D. Bartle, C.L. Woolley, K.E. Markides, M.L. Lee, R.S. Hansen, Rayleigh instability of stationary phase films in capillary column chromatography, J. High Resolut. Chromatogr. 10 (1987) 128–136. https://doi.org/10.1002/jhrc.1240100305.
[21] H.L. Ngo, K. LeCompte, L. Hargens, A.B. McEwen, Thermal properties of imidazolium ionic liquids, Thermochim. Acta 357–358 (2000) 97–102. https://doi.org/10.1016/S0040-6031(00)00373-7.
[22] Y. Cao, T. Mu, Comprehensive investigation on the thermal stability of 66 ionic liquids by thermogravimetric analysis, Ind. Eng. Chem. Res. 53 (2014) 8651–8664. https://doi.org/10.1021/ie5009597.
[23] D.M. Blake, L. Moens, D. Rudnicki, H. Pilath, Lifetime of imidazolium salts at elevated temperatures, J. Sol. Energy Eng. 128 (2006) 54–57. https://doi.org/10.1115/1.2148976.
[24] Y. Huang, Z. Chen, J.M. Crosthwaite, S. N.V.K. Aki, J.F. Brennecke, Thermal stability of ionic liquids in nitrogen and air environments, J. Chem. Thermodyn. 161 (2021) 106560. https://doi.org/10.1016/j.jct.2021.106560.
[25] A.S. Amarasekara, O.S. Owereh, Thermal properties of sulfonic acid group functionalized Brönsted acidic ionic liquids, J. Therm. Anal. Calorim. 103 (2011) 1027–1030. https://doi.org/10.1007/s10973-010-1101-5.
[26] R.L. Levy, H.D. Gesser, T.S. Herman, F.W. Hougen, Application of column bleed absorption in high sensitivity gas chromatography and in gas chromatography-mass spectrometry, Anal. Chem. 41 (1969) 1480–1483. https://doi.org/10.1021/ac60280a041.
[27] A. Sala, F. Ferrario, E. Rizzi, S. Catinella, P. Traldi, Electron ionization mass spectrometry of some 1-and 2-alkylimidazoles and 1,3-dialkylimidazole iodides, Rapid Commun. Mass Spectrom. 6 (1992) 388–393. https://doi.org/10.1002/rcm.1290060607.
[28] Y. Chen, Y. Cao, Y. Shi, Z. Xue, T. Mu, Quantitative research on the vaporization and decomposition of [EMIM][Tf_2N] by thermogravimetric analysis–mass spectrometry, Ind. Eng. Chem. Res. 51 (2012) 7418–7427. https://doi.org/10.1021/ie300247v.

[29] A. Deyko, K.R.J. Lovelock, P. Licence, R.G. Jones, The vapour of imidazolium-based ionic liquids: a mass spectrometry study, Phys. Chem. Chem. Phys. 13 (2011) 16841. https://doi.org/10.1039/c1cp21821b.
[30] K.R.J. Lovelock, J.P. Armstrong, P. Licence, R.G. Jones, Vaporisation and thermal decomposition of dialkylimidazolium halide ion ionic liquids, Phys Chem Chem Phys 16 (2014) 1339–1353. https://doi.org/10.1039/C3CP52950A.
[31] C. Neise, C. Rautenberg, U. Bentrup, M. Beck, M. Ahrenberg, C. Schick, O. Keßler, U. Kragl, Stability studies of ionic liquid [EMIm][NTf_2] under short-term thermal exposure, RSC Adv. 6 (2016) 48462–48468. https://doi.org/10.1039/C6RA06129J.
[32] M.T. Clough, K. Geyer, P.A. Hunt, J. Mertes, T. Welton, Thermal decomposition of carboxylate ionic liquids: trends and mechanisms, Phys. Chem. Chem. Phys. 15 (2013) 20480. https://doi.org/10.1039/c3cp53648c.
[33] R.A. Patil, M. Talebi, A. Berthod, D.W. Armstrong, Dicationic ionic liquid thermal decomposition pathways, Anal. Bioanal. Chem. 410 (2018) 4645–4655. https://doi.org/10.1007/s00216-018-0878-0.
[34] H. Ohtani, S. Ishimura, M. Kumai, Thermal decomposition behaviors of imidazolium-type ionic liquids studied by pyrolysis-gas chromatography, Anal. Sci. 24 (2008) 1335–1340. https://doi.org/10.2116/analsci.24.1335.
[35] M. Sawada, Y. Takai, C. Chong, T. Hanafusa, S. Misumi, Pyridinium ion reactivities: Substituent effect on the reverse menschutkin reaction of l-methylpyridinium cations with iodide anion, Tetrahedron Letters 26 (1985) 5065–5068. https://doi.org/10.1016/S0040-4039(01)80854-6.
[36] B. Chan, N. Chang, M. Grimmett, The synthesis and thermolysis of imidazole quaternary salts, Aust. J. Chem. 30 (1977) 2005. https://doi.org/10.1071/CH9772005.
[37] M. Mahrova, M. Conte, E. Roman, R. Nevshupa, Critical insight into mechanochemical and thermal degradation of imidazolium-based ionic liquids with alkyl and monomethoxypoly(ethylene glycol) side chains, J. Phys. Chem. C 118 (2014) 22544–22552. https://doi.org/10.1021/jp504946h.
[38] W.H. Awad, J.W. Gilman, M. Nyden, R.H. Harris, T.E. Sutto, J. Callahan, P.C. Trulove, H.C. DeLong, D.M. Fox, Thermal degradation studies of alkyl-imidazolium salts and their application in nanocomposites, Thermochim. Acta 409 (2004) 3–11. https://doi.org/10.1016/S0040-6031(03)00334-4.
[39] S.C. Dhanesar, M.E. Coddensr, C.F. Poole, Surface roughening by sodium chloride deposition for the preparation of organic molten salt open tubular columns, J. Chromatogr. Sci. 23 (1985) 320–324. https://doi.org/10.1093/chromsci/23.7.320.
[40] W. Mei, A. Han, R.J. Hickey, R.H. Colby, Effect of chemical substituents attached to the zwitterion cation on dielectric constant, J. Chem. Phys. 155 (2021) 244505. https://doi.org/10.1063/5.0074100.
[41] J.L. Anderson, D.W. Armstrong, High-stability ionic liquids. A new class of stationary phases for gas chromatography, Anal. Chem. 75 (2003) 4851–4858. https://doi.org/10.1021/ac0345749.
[42] I. Grossereid, K.C. Lethesh, V. Venkatraman, A. Fiksdahl, New dual functionalized zwitterions and ionic liquids; Synthesis and cellulose dissolution studies, J. Mol. Liq. 292 (2019) 111353. https://doi.org/10.1016/j.molliq.2019.111353.
[43] A. Efimova, J. Varga, G. Matuschek, M.R. Saraji-Bozorgzad, T. Denner, R. Zimmermann, P. Schmidt, Thermal resilience of imidazolium-based ionic liquids—studies

on short- and long-term thermal stability and decomposition mechanism of 1-alkyl-3-methylimidazolium halides by thermal analysis and single-photon ionization time-of-flight mass spectrometry, J. Phys. Chem. B 122 (2018) 8738–8749. https://doi.org/10.1021/acs.jpcb.8b06416.

[44] F.W. McLafferty, Mass spectrometric analysis. Molecular rearrangements, Anal. Chem. 31 (1959) 82–87. https://doi.org/10.1021/ac60145a015.

[45] J.H. Gross, Fragmentation of Organic Ions and Interpretation of EI Mass Spectra, in: Mass Spectrom., Springer Berlin Heidelberg, Berlin, Heidelberg, 2011: pp. 249–350. https://doi.org/10.1007/978-3-642-10711-5_6.

[46] F.W. McLafferty, Interpretation of Mass Spectra, third, University Science Books, Mill Valley, California, 1980.

[47] E. Thomas, D. Thomas, K.P. Vijayalakshmi, B.K. George, Mechanistic outlook on thermal degradation of 1,3-dialkyl imidazolium ionic liquids and organoclays, RSC Adv. 6 (2016) 9421–9428. https://doi.org/10.1039/C5RA24907D.

[48] R.P. Lattimer, Mass spectral analysis of low-temperature pyrolysis products from poly(tetrahydrofuran), J. Anal. Appl. Pyrolysis 57 (2001) 57–76. https://doi.org/10.1016/S0165-2370(00)00106-6.

Figure Legends

Figure 1. Chemical structures of the ZIL stationary phases synthesized and evaluated in this study.

Figure 2. Breakdown of ZIL chemical structure based on cation and anion system and additional terminology referenced throughout the manuscript.

Figure 3. Bleed diagrams of ZIL stationary phases acquired using GC-MS. T_{bleed} was determined to be the temperature at which the bleed profile reached 10^6 counts, an approximate order of magnitude increase in counts from the baseline. Values for T_{bleed} are listed for each ZIL.

Figure 4: Proposed thermal degradation mechanism of oligoether ZIL stationary phases.

Figure 5. Proposed thermal degradation mechanisms of sulfonate and triflimide ZIL stationary phases.

696 Table 1. GC conditions for isothermal separations

Conditions	
Inlet Temperature	250 °C
Flow Rate	1 mL min^{-1}
Oven Temperature	100 °C
Carrier Gas	Helium
FID Temperature	250 °C
Air Flow	395 mL min^{-1}
Fuel Flow	35 mL min^{-1}
Makeup Flow	25 mL min^{-1}

697

698 Table 2. GC conditions for MAOT column baking at 125, 150, 175, 200, 225, and 250 °C

Conditions	
Inlet Temperature	250 °C
Flow Rate	1 mL min^{-1}
Oven Temperature	100 °C to 125 °C @ 20 °C min^{-1} (hold 1 h) back to 100 °C @ 20 °C min^{-1}
Carrier Gas	Helium
FID Temperature	250 °C
Air Flow	300 mL min^{-1}
Fuel Flow	40 mL min^{-1}
Makeup Flow	25 mL min^{-1}

699

700 Table 3. List of ZIL stationary phases, including abbreviations, physical descriptions, densities
701 and melting points.

Abbreviation	Description	Density[a] (g mL^{-1})	Melting Point (°C)
C_8ImC_3S	Viscous clear liquid	1.14 ± 0.05	RTIL
$C_{10}ImC_3S$	White waxy solid	1.14 ± 0.06	85-87
OE_2ImC_3S	Viscous clear liquid with slight yellow tint	1.27 ± 0.09	RTIL
OE_3ImC_3S	Viscous clear liquid with slight yellow tint	1.21 ± 0.08	RTIL
$OE_3(Ph)ImC_3S$	White crystalline solid	1.38 ± 0.08	92-98
$C_8(Ph)ImC_3S$	White crystalline solid	n.d.	T.D.
C_8ImC_2S	Viscous clear liquid	n.d.	RTIL
C_8ImC_3NTf	White crystalline solid	1.22 ± 0.06	91-93

702 [a] pycnometer method at 20-21 °C; n.d. not determines; T.D. thermally degraded at 190 °C

Table 4. Maximum allowable operating temperature (MAOT) values for alkyl and oligoether substituted ZILs on untreated and salt-deactivated capillary.

Phase	Rearrangement Temperatures	Thermal Degradation Temperature[a]
C_8ImC_3S	125-225 °C	225-250 °C[b]
C_8ImC_3S-Salt	n.r.	200-225 °C
$C_{10}ImC_3S$	125-225 °C	225-250 °C[b,c]
C_8ImC_3NTf	≤ 100 °C	n.d.
OE_2ImC_3S	150-200 °C	200-225 °C
OE_3ImC_3S	≤ 100 °C	n.d.
OE_3ImC_3S-Salt	150-200 °C	200-225 °C[b]
$OE_3(Ph)ImC_3S$	100-175 °C	175-200 °C

[a] Thermal degradation temperature range indicates the temperature before and at which the retention factor of benzyl alcohol or propionic acid dropped by more than 2% from the initial value.

[b] Temperature ranges are based on the results of propionic acid instead of benzyl alcohol.

[c] For the $C_{10}ImC_3S$ ZIL column, retention factors were observed to increase for both benzyl alcohol and propionic acid after heating, so MAOT may be higher than the true value.

n.r. no rearrangement was observed

n.d. not determined due to significant phase rearrangement at 100 °C

713 Table 5. Molecular ions and their fragments obtained from bleed profiles at 411-412 min (245.5-
714 246 °C).

ZIL Phase	Molecular Ion (m/z)	Molecular Ion Fragments (m/z)
C_8ImC_3S	C_8Im (m/z 180)	179, 165, 153, 151, 137, 123, 109, 96, 95, 82, 81, 69, 68
	C_1Im (m/z 82)	55
	1-chlorooctane (m/z 134)	107, 105, 93, 91
$C_{10}ImC_3S$	$C_{10}Im$ (m/z 208)	207, 193, 181, 179, 165, 151, 137, 123, 109, 96, 95, 82, 81, 69, 68, 67
C_8ImC_3NTf	$C_8ImC_3NTf\text{-}CF_3$ (m/z 364)	184, 180
	C_8Im (m/z 180)	179, 165, 153, 151, 137, 123, 109, 95, 81, 54
	$C{=}C_2NTf$ (m/z 253)	184, 133, 120, 69
C_8ImC_2S	C_8Im (m/z 180)	179, 165, 153, 151, 137, 123, 109, 95, 71, 57
	1-bromooctane (m/z 192)	194, 151, 149, 137, 135, 109, 107, 71, 57
	1-octene (m/z 112)	97, 83, 69, 57, 55
OE_2ImC_3S	OE_2Im (m/z 170)	169, 155, 139, 138, 125, 111, 95, 94, 89, 81, 68, 67, 59, 58
	$C_7H_{12}N_2O$ (m/z 140)	111, 95, 81, 73, 67, 59
	$C_5H_8N_2O$ (m/z 112)	95, 94, 81, 67
	$C_5H_8N_2$ (m/z 96)	69, 67
	C_1Im (m/z 82)	55
	$C_2H_4SO_3$ (m/z 108)	108
OE_3ImC_3S	OE_3Im (m/z 214)	213, 199, 183, 169, 155, 139, 125, 124, 111, 95, 94, 89, 81, 67, 59
	$C_7H_{12}N_2O_2$ (m/z 156)	138, 125, 111, 95, 94, 89, 81, 67
	$C_6H_{10}N_2O$ (m/z 126)	95, 94, 81, 67, 59
	$C_5H_8N_2O$ (m/z 112)	95, 94, 81, 67
	$C_5H_8N_2$ (m/z 96)	69, 67
	C_1Im (m/z 82)	55
$OE_3(Ph)ImC_3S$	$OE_3(Ph)Im$ (m/z 290)	275, 259, 245, 232, 215, 213, 201, 187, 171, 170, 157, 143, 103, 89, 77, 59
	$C_{13}H_{16}N_2O_2$ (m/z 232)	215, 214, 201, 187, 171, 170, 157, 143, 89, 77
	$C_{12}H_{14}N_2O$ (m/z 202)	171, 170, 157, 143, 77, 59
	$C_{11}H_{12}N_2O$ (m/z 188)	170, 157, 143, 77
	$C_{11}H_{10}N_2O$ (m/z 186)	157, 143, 77
	$C_{11}H_{12}N_2$ (m/z 172)	143, 77
	$C_{10}H_{10}N_2$ (m/z 158)	77, 55
	PhIm (m/z 144)	117, 116, 77
	$C_5H_{12}O_2$ (m/z 104)	59
$BzImC_3S$	BzIm (m/z 158)	91, 77, 65
Anion system	1,3-propanesultone (m/z 122)	58, 57

715

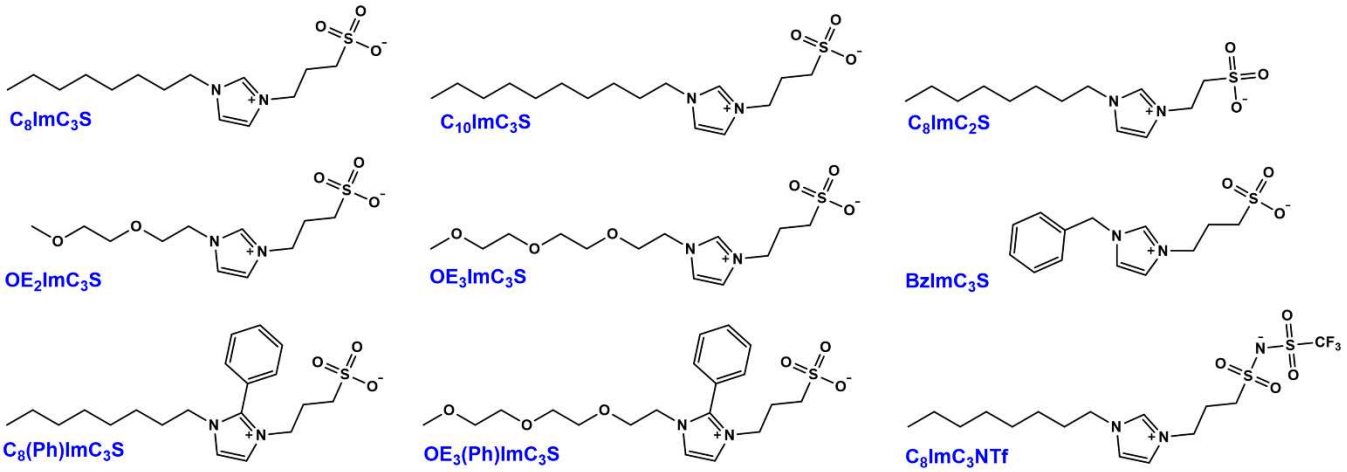

716

717 Figure 1. Chemical structures of the ZIL stationary phases synthesized and evaluated in this
718 study.

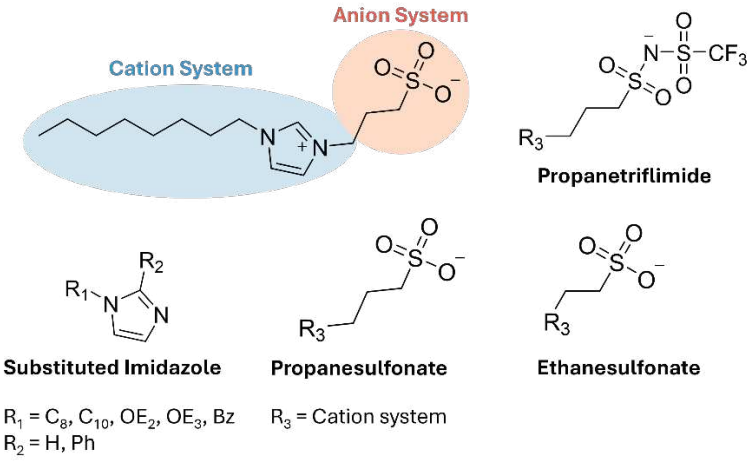

719

720 Figure 2. Breakdown of ZIL chemical structure based on cation and anion system and additional
721 terminology referenced throughout the manuscript.

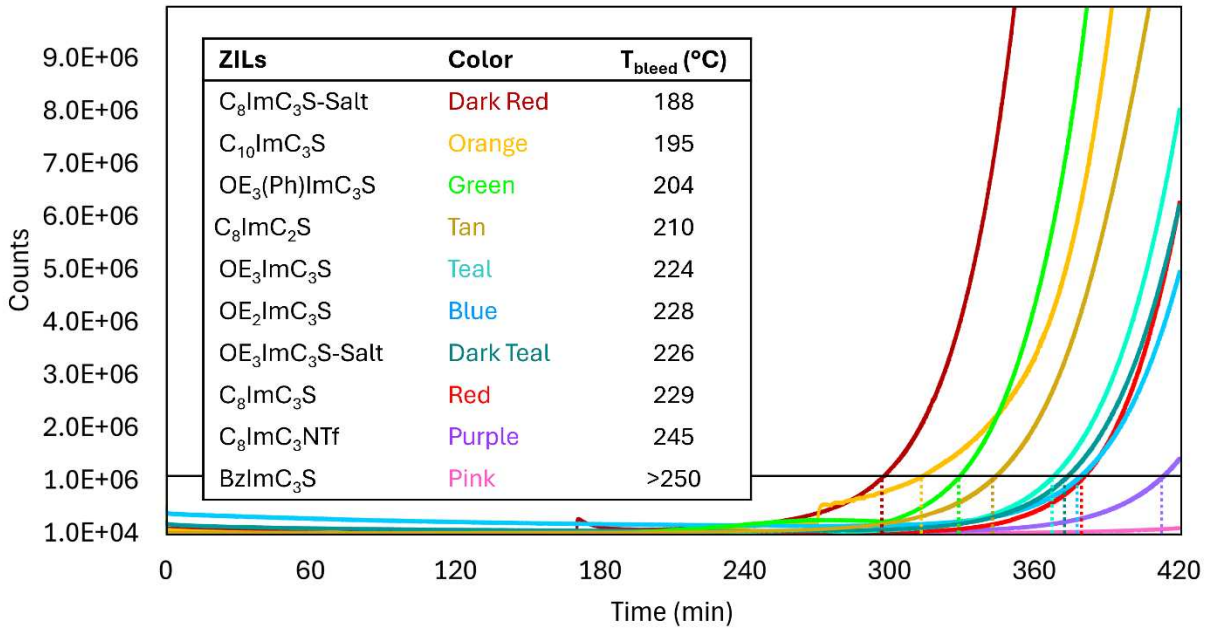

722

723 Figure 3. Bleed diagrams of ZIL stationary phases acquired using GC-MS. T_{bleed} was determined
724 to be the temperature at which the bleed profile reached 10^6 counts, an approximate order of
725 magnitude increase in counts from the baseline. Values for T_{bleed} are listed for each ZIL.

726

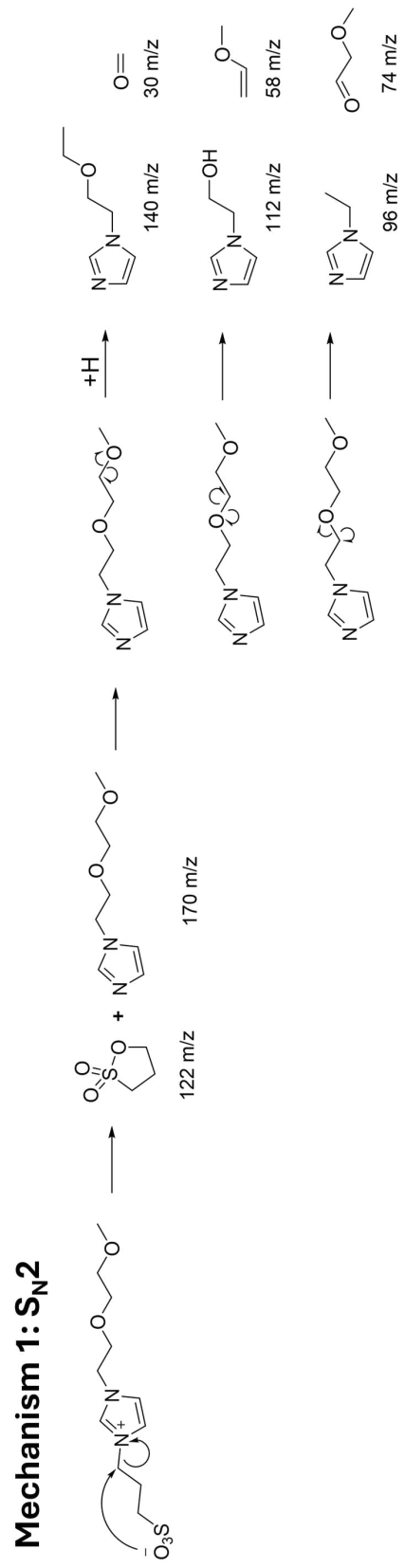

Figure 4: Proposed thermal degradation mechanism of oligoether ZIL stationary phases.

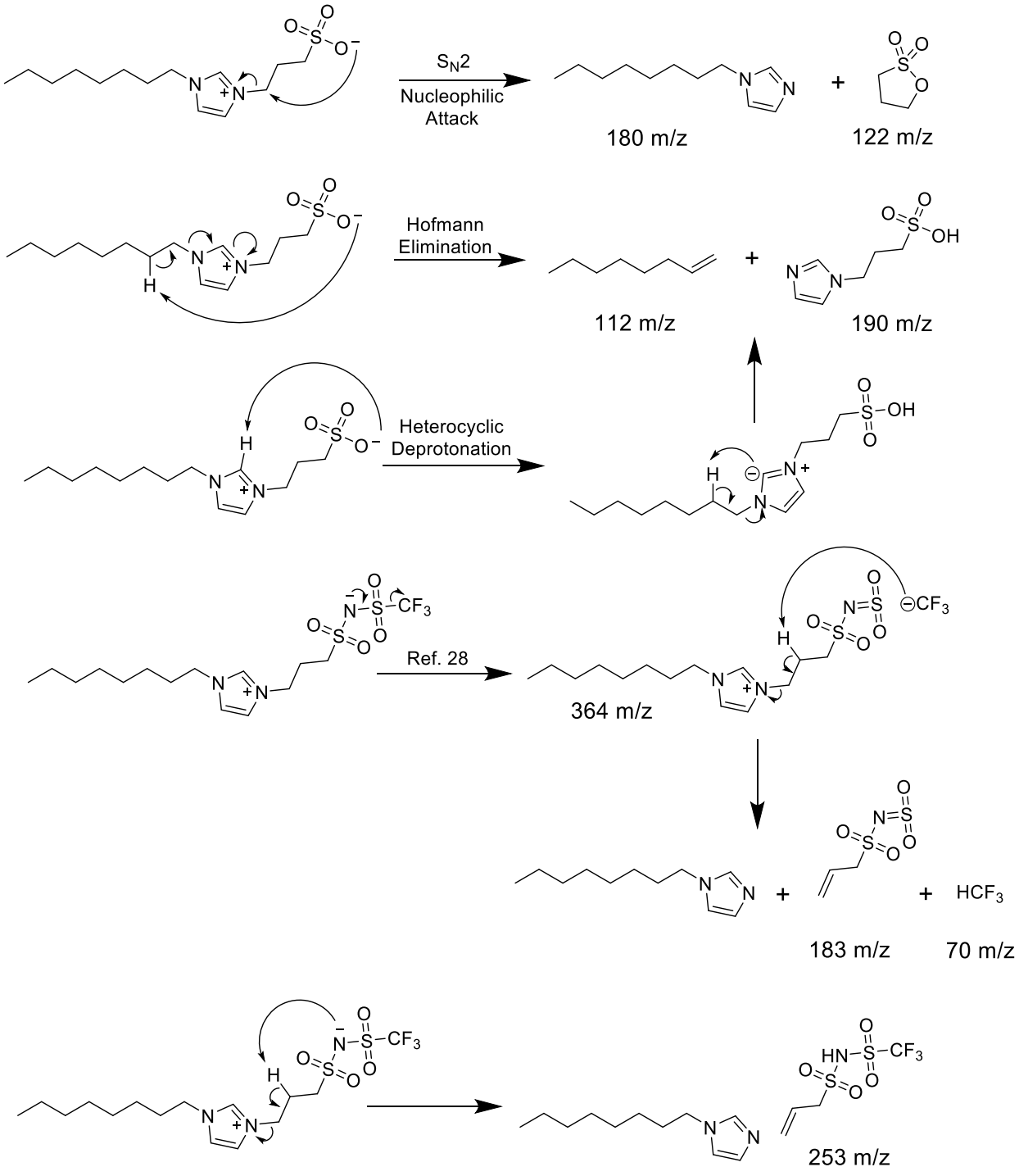

Figure 5. Proposed thermal degradation mechanisms of sulfonate and triflimide ZIL stationary phases.